



ASME Accepted Manuscript Repository

Institutional Repository Cover Sheet

First

Last

ASME Paper Title: New methodology for optimal placement of piezoelectric sensor/actuator pairs for active vibration control of flexible structures

Authors: Ali H Daraji, Jack M Hale and Jianqiao Ye

ASME Journal Title: Journal of Vibration and Acoustics

Volume/Issue 140 (1)

Date of Publication (VOR* Online) 29th September 2017

ASME Digital Collection URL: <http://vibrationacoustics.asmedigitalcollection.asme.org/article.aspx?articleid=264818>

DOI: 10.1115/1.4037510

*VOR (version of record)

New methodology for optimal placement of piezoelectric sensor/actuator pairs for active vibration control of flexible structures

Ali H. Daraji¹

Engineering Department, Lancaster University, UK

e-mail: a.daraji@lancaster.ac.uk

ASME Membership (102081192)

Jack M. Hale

School of Mechanical and Systems Engineering, Newcastle University, UK

e-mail: jack.hale@ncl.ac.uk

Jianqiao Ye*

Engineering Department, Lancaster University, UK

e-mail: j.ye2@lancaster.ac.uk

ABSTRACT

This paper describes a computationally efficient method to determine optimal locations of sensor/actuator (s/a) pairs for active vibration reduction of a flexible structure. Previous studies have tackled this problem using heuristic optimization techniques achieved with numerous combinations of s/a locations and converging on a suboptimal or optimal solution after multi thousands of generations. This is computationally expensive and directly proportional to the number of sensors, actuators, possible locations on structures and the number of modes required to be suppressed (control variables). The current work takes a simplified approach of modeling a structure with sensors at all locations, subjecting it to external excitation force or structure base excitation in various modes of interest and noting the locations of n sensors giving the largest average percentage sensors effectiveness. The percentage sensor effectiveness is measured by dividing all sensor output voltage over the maximum for each mode using time and frequency domain analysis. The methodology was implemented for dynamically symmetric and asymmetric structures under external force and structure base excitations to find the optimal distribution based on time and frequency responses analysis. It was found that the optimized sensor

*Corresponding author

locations agreed well with the published results for a cantilever plate, while with very much reduced computational effort and higher effectiveness. Furthermore, it was found that collocated s/a pairs placed in these locations offered very effective active vibration reduction for the structure considered.

Keywords, vibration control, optimal location, piezoelectric sensor, sensor effectiveness, base excitation

1. INTRODUCTION

High specific strength structures used in modern aerospace and other applications have low inherent damping which can lead to vibration problems. In these applications the conventional solution of adding high damping coatings is not appropriate because of the significant added mass. Hence, an alternative vibration control technique, such as Active Vibration Control (AVC), is desirable. AVC uses a number of actuators to apply oscillating forces (sometimes rather misleadingly known as “anti-vibration”) to reduce the vibration. This requires sensors to measure the vibration and a controller to generate output to the actuators with appropriate magnitude, frequency and phase, based on the input from the sensors. Sensors and actuators are normally collocated to eliminate the problem of “modal spill-over”, but for structures of even moderate complexity subject to vibration in multiple modes it is not obvious where these s/a pairs should be located for best effect.

Many studies have paid attention to using discrete point piezoelectric sensor, actuator and their locations to optimize vibration reduction, though lower sensing and control effects were expected from a full coverage structure with a single layer sensor and actuator [1-3]. Kumar and Narayanan addressed that the placement of sensors and actuators had an important effect on the control system performance and misplaced sensors and actuators led

to problems such as lack of system observability and controllability [4]. A method was presented by Kondoh et al to optimize locations of sensors, actuators and feedback gain based on minimization of the quadratic cost function using simple search by testing seven locations on a cantilever beam [5]. The optimal placement and sizing of a single piezoelectric actuator proposed by Devasia et al was also based on minimization of a quadratic cost function implemented for a simply supported beam using a simple numerical search algorithm [6].

Several methodologies have been developed to determine the optimal locations of a limited number of sensors and actuators on structures of limited complexity such as beams, plates and shells, based on heuristic search algorithms such as the genetic algorithms [7-12]. The optimization of feedback gain and three s/a pairs for suppression of the first four modes of a cantilever beam were investigated by Zhang et al, taking the maximization of energy dissipation as the objective function [7]. Sadri et al investigated vibration reduction of a simply supported plate by optimally placing two actuators based on modal controllability and controllability gramian as objective functions [8]. The placement of two actuators and six piezofilm sensors was studied by Han and Lee for a cantilever plate based on gramian controllability and observability to suppress the first five modes of vibration [9]. Peng used maximization of the gramian controllability as the objective function to optimize the placement of four s/a pairs to attenuate the first five modes of vibration [10]. A computational scheme using spatial H_2 norm was proposed by Liu et al to optimize the locations of four sensors and actuators on a clamped-clamped plate [11]. Bruant et al investigated the optimal position and orientation of sensors and actuator for simply supported plate [12].

Limited studies have proposed a placement methodology using intelligent swarm evolution algorithms to optimize the locations of sensors and actuators [13-15], and

implemented the approach for a simply supported plate to locate two piezoelectric sensors and actuators [13], an aircraft fin-tip to optimize three piezoelectric actuators and accelerometer sensors [14], and a cantilever beam to place two piezoelectric s/a pairs [15].

Though, the above published studies investigated small-scale structures to optimize a small number of sensors and actuators with limited possible locations on a structure, the search space of the optimization problem for such structures contained numerous combinations of s/a pairs and exhaustive search to find the optimal solution is computationally prohibitive. Therefore genetic and intelligent swarm algorithms have been used to find the optimal or suboptimal solution and shown to be superior in computation effort and accuracy compared to the exhaustive search method. The computational effort of the evolution search algorithms is exponentially increased with number of control variables and, as reported by Darivandi et al, the existing optimization schemes for optimal sensor and actuator placement may be inaccurate or computationally impractical [16]. A simplified procedure to find the optimal distribution of sensors and actuators for small and large-scale structures with low computational effort is highly desirable.

In this study, a new and simpler methodology is developed to determine the unique global optimal distribution of piezoelectric s/a pairs on flexible structures for active vibration control. It is proposed that these optimal sites will be the locations where sensors will generate maximum output voltage when the structure is driven into the resonant modes. To test this new method, symmetric and asymmetric plates covered with small piezoelectric sensors are modelled using the ANSYS finite element package. The voltage outputs from all these sensors are obtained when the plates are driven at resonance frequencies. The best

locations identified by the current approach are compared with published optimal s/a locations.

2. MODELING

In this study, it was assumed that the structural mass, stiffness and damping coefficient were constant over the time, and the structure model was liner elastic. Non-coupled modal dynamic equations in state space formed for a flexible linear elastic structure with discrete piezoelectric sensors and actuators bonded to its surface are as follows [3]:

$$\dot{X} = \begin{bmatrix} 0 & \omega \\ -\omega & -2\xi\omega \end{bmatrix} X + \begin{bmatrix} 0 \\ \varphi^T \end{bmatrix} F_d + \begin{bmatrix} 0 \\ -\varphi^T K_{u\phi}^a \end{bmatrix} \phi_a \quad (1)$$

$$\dot{X} = AX + B\phi_a + B_{md}F_d \quad , \quad \phi_s = CX \quad (2)$$

$$X = \begin{Bmatrix} \omega\eta \\ \dot{\eta} \end{Bmatrix} \quad , \quad \dot{X} = \begin{Bmatrix} \dot{\eta} \\ \ddot{\eta} \end{Bmatrix} \quad (3)$$

where A , B , C , B_{md} and $K_{u\phi}$ are state, actuator, sensor, external disturbance and piezoelectric coupling matrices, respectively. State and external force disturbance vectors are denoted by X and F_d . An open-loop mass-normalised modal matrix obtained by solving the free vibration problem of an undamped structure is denoted by φ for each fundamental frequency ω , and η is a single vector of the modal coordinates. Sensor output and actuator feedback voltages are denoted by ϕ_s and ϕ_a . The structural damping ratio ξ as a result of the stiffness and mass of the structure was assumed to be low and equal to 0.002 for all the structures used in this study.

$$A_i = \begin{bmatrix} 0 & \omega_i \\ -\omega_i & -2\xi_i\omega_i \end{bmatrix} \quad , \quad B_i = \begin{bmatrix} 0 \\ -\varphi^T K_{u\phi}^a \end{bmatrix} \quad (4)$$

$$B_{mdi} = \begin{bmatrix} 0 \\ \varphi_i^T \end{bmatrix}, \quad C_i = [-\varphi_i^T \omega_i^{-1} C_p^{-1} K_{u\phi}^s \quad 0] \quad (5)$$

$$X_i = \{\omega_i \eta_i \quad \dot{\eta}_i\}^T \quad (6)$$

where A_i , B_i , B_{mdi} , C_i and X_i are individual modal state, input actuator, mechanical external disturbance, output sensor matrix and state vector, respectively. The subscripts i , s and a refer to the i^{th} mode, sensor and actuator, respectively. Piezoelectric capacitance is denoted by C_p . The state matrices for n_m modes and r_a actuators are given by:

$$A_{(2n_m \times 2n_m)} = \begin{bmatrix} A_1 & \cdots & 0 \\ \vdots & \ddots & \vdots \\ 0 & \cdots & A_{n_m} \end{bmatrix} \quad (7)$$

$$B_{(2n_m \times r_a)} = \begin{bmatrix} (B_1)_{r_a} & \cdots & (B_1)_{r_a} \\ \vdots & \cdots & \vdots \\ (B_{n_m})_{r_a} & \cdots & (B_{n_m})_{r_a} \end{bmatrix} \quad (8)$$

$$C_{(r_a \times 2n_m)} = \begin{bmatrix} (C_1)_{r_a} & \cdots & (C_{n_m})_{r_a} \\ \vdots & \cdots & \vdots \\ (C_1)_{r_a} & \cdots & (C_{n_m})_{r_a} \end{bmatrix} \quad (9)$$

$$X_{(2n_m \times 1)} = \{\omega_1 \eta_1 \quad \dot{\eta}_1 \quad \cdots \quad \omega_{n_m} \eta_{n_m} \quad \dot{\eta}_{n_m}\}^T \quad (10)$$

3. CONTROL SCHEME

Feedback control gain was determined to suppress plate vibration using the optimal linear quadratic control scheme. This control scheme is based on the minimization of the performance index J [17]:

$$J = \int_0^{\infty} (X^T Q X + \phi_a^T R \phi_a) dt \quad (11)$$

The weighting matrix Q of dimensions $2n_m \times 2n_m$ and R of dimensions $r_a \times r_a$ are diagonal and positive definite, where n_m and r_a are the number of modes that are required to be suppressed and the number of actuators paired to sensors. The level of vibration reduction and the required external energy to suppress vibration are directly proportional to the values of the elements in the Q matrix. The derivation of the optimal linear controller leads to the following Riccati equation [17]:

$$A^T P + PA - PBR^{-1}B^T P + Q = 0 \quad (12)$$

$$K = R^{-1}B^T P, \quad \phi_a = -KX \quad (13)$$

For a given control system, all the parameters of the Reduced Riccati equation (12) are known, from which matrix P can be solved. The control system is stable or the closed loop control is stable if the trace of matrix P is positive definite. Controller gain is obtained after substitution of matrix P in equation (13). In this study, the optimal actuator matrix B was determined by pairing actuators with optimal sensor locations to get optimal controller feedback gain K and actuator feedback voltage ϕ_a from equation (13).

4. COMPLEXITY OF PIEZOELECTRIC PLACEMENT

The challenge of optimal placement of sensors and actuators on flexible structures increases with the surface area of the structure, the number of possible locations on the structure, the number of sensors and actuators to be optimized and the number of vibration modes to be suppressed. The number of possible combinations of r locations from n possibilities is given by:

$$C(n, r) = \frac{n!}{r!(n-r)!} \quad (14)$$

For 490 mm square plate discretised into one hundred possible sites, it is obvious that there are one hundred places to locate a single sensor (100 combinations) and only one combination for placing one hundred sensors (one in every location). The number of combinations rises greatly between these extremes as shown in Figure 1 with a maximum of 10^{29} combinations of locations for 50 sensors. Even ten sensors have 1.73×10^{13} combinations, as shown by equation (14). It is clearly impractical to evaluate the effectiveness of every possibility. For this reason, guided search techniques, such as the genetic algorithm are used to find the optimal solution, though this is still impractical for large possible combinations.

The level of the problem's complexity in most published works investigating the optimal locations of sensors and actuators for small beam, plate and shell structures using genetic algorithms are located in the shaded area shown in Figure 1(b). Darivandi et al reported that the existing optimization schemes for optimal piezoelectric placement may be inaccurate or computationally impractical using genetic algorithm [16]. The issue of extremely large candidate solutions using genetic algorithms was addressed by Papadimitriou to optimize sensor locations for parametric identification structural system [18]. The genetic algorithms program was run twenty thousand cycles of calculation for five times to find the optimal locations of four sensors and actuators on a small plate [11] and fifty thousand generations to locate six sensors [9].

In this study, the optimal configuration of full coverage segmented piezoelectric sensors is proposed to reduce the number of iterations to just one cycle, i.e., when r is equal to n , in

equation (14). The proposed method reduces the number of candidate solutions to just one bonded piezoelectric element during the test. This elimination in candidate solutions reduces the computational effort to just one cycle calculation and holds great potential to solve both small and large-scale structures.

5. PIEZOELECTRIC PLACEMENT METHODOLOGY

The methodology is implemented by covering the entire surface of a flexible structure with discrete piezoelectric sensors subjected to an external excitation force or structure base excitation at frequencies coinciding with the structural natural frequencies. An ANSYS Parametric Design Language (APDL) programme is developed using the three-dimensional solid45 finite element for the passive structure and solid5 for sensors. The optimal sensor configuration is determined based on the sensor output voltage and their percentage effectiveness with respect to other sensors under multiple modes of vibration. The application of this method has the following steps.

1. An external excitation force oscillating in the plate thickness direction at the first n_m modes required to be suppressed is applied at a point of large amplitude on the structure (external force excitation), or by exciting the mounting edges of a structure at the resonant modes (base excitation). An APDL program is developed to investigate the open loop output voltage time or frequency responses of all sensors.
2. The percentage effectiveness of sensors are found at each mode of vibration by dividing the absolute voltage of the sensors over the maximum absolute according to the following equation:

$$S_{i,j} = \frac{|\phi_{s_{i,j}}|}{|\phi_{sm_j}|} 100\% \quad \text{where } i = 1,2,3 \dots n_s, j = 1,2,3 \dots n_m \quad (15)$$

S : sensor effectiveness

ϕ_s : sensor voltage at transient or steady state for time domain analysis or peak sensor voltage for frequency domain analysis

ϕ_{sm} : maximum voltage value for all sensors

Subscripts i and j are sensor and mode number, respectively

n_s : total number of sensors

n_m : total number of modes to be investigated

3. The average percentage effectiveness is calculated for all modes of vibration as follows:

$$AS_i = \frac{1}{n_m} \sum_{j=1}^{n_m} \beta_j S_{i,j} \quad (16)$$

AS : average sensor effectiveness

n_m : total number of modes to be investigated

β : mode weighting factor

4. The optimal sensor locations are ranked in a descending order according to the average percentage effectiveness calculated in the previous step.
5. The number of the active s/a pairs at each mode is determined according to equation (17). This number is less than the total number of piezoelectric pairs required to be optimized to suppress number of modes.

$$\gamma_j = \sum_{i=1}^{n_{sa}} S_{i,j} \quad (17)$$

$$i = 1 \text{ or } 2 \text{ or } 3 \dots \text{or } n_s, \quad j = 1 \text{ or } 2 \text{ or } 3 \dots \text{or } n_m$$

Where γ_j is the number of active s/a pairs at mode number j , the sensor percentage effectiveness value $S_{i,j}$ is taken for the optimal sensor locations or the largest values.

The total active sensor/actuator pairs to suppress all the required modes of vibration is higher than the number of s/a pairs required to be optimized and can be determined according to the following equation:

$$\gamma = \sum_{i=1}^{n_m} \gamma_j \quad (18)$$

6. RESEARCH PROBLEM

The above placement methodology was implemented to investigate the optimal placement for three types of cantilever plates shown in Figure 2 that have different geometry and boundary conditions. The type-I cantilever plate has symmetric geometry and boundary conditions, and has one axis of symmetry. This plate was selected to test the methodology and to validate the results with the published work. The other two cantilever plates, (type-II) and geometry (type-III), are more complex and dynamically asymmetrical due to the plate boundary conditions. The plates were tested under external excitation force applied at the point of large amplitude and structure base excitations using time and frequency domain analysis. The properties of the plates and the piezoelectric sensor material are listed in Table 1.

7. RESULTS AND DISCUSSION

7.1 Natural frequencies

The first six natural frequencies for the symmetrical and asymmetrical plates were determined taking account of the added mass and stiffness of the piezoelectric sensors. The results are shown in Table 2. It is clear that the effect of boundary conditions and beam

stiffeners have resulted in an increase in the plate stiffness and the natural frequencies. An accurate calculation of the natural frequencies is important, since the method requires an external force and base excitation at the structure's resonance frequencies for the time and frequency domain analyses.

7.2 Comparison of time and frequency domain analysis

According to the methodology explained in Section 5, the type-I smart plate shown in Figure 2 was subjected to an external excitation force normal to the plate at the free end when the first six natural frequencies were considered. APDL programming was built to investigate the open loop voltage time and frequency domain analyses for all sensors. Data were captured for all sensors to show the distribution of the average electrical voltage generated in the piezoelectric sensors, as shown in Figure 3. Sensors voltage time domain analyses at the steady state for the first, second and the fifth modes are shown on the left hand side of Figure 3 and the frequency domain analyses are shown on the right hand side. It can be observed that the electric voltage is distributed symmetrically about the plate's axis of symmetry, and varied from positive to negative for most modes of vibration. This variation highlights the importance of the segmented sensor electrode and sensor dimensions in preventing cancellation of sensor output voltage over a large area of sensors. Also, the sensors located at the root of the cantilever plate are active, sensitive and produce higher voltage than others for most modes of vibration.

Figure 3 shows a comparison study between sensor output voltage time and frequency responses. It can be observed from this comparison that the distributions of sensor voltage over the plate surface are the same from both analyses. It was noticed that the computation

effort for the sensor voltage frequency analysis was much lower than the time response analysis at steady state.

At the first mode, Figures 3 and 4 show that the distribution of the sensor voltage at the transient response of time domain analysis is similar to the distribution at the steady state and frequency domain analysis. It was found that the computation time for the determination of the percentage sensor effectiveness at the first mode for time domain analysis at transient zone was greatly reduced to (35.1 s) compared to the steady state (92431.4 s), but the computational effort at frequency domain analysis (26 s) is more efficient than time domain analysis. This comparison highlights flexibility of the method and validates the results.

The optimal sensor locations required to suppress a single mode of vibration can be directly placed at locations of maximum output sensor voltage, but for multiple modes of vibration and complex structures an efficient methodology is required to find optimal sensor locations as explained in Section 5. The percentage effectiveness was calculated for all sensors for each mode and the average was taken for all modes with unity mode weighting factors according to Steps 2 and 3 in Section 5. The results were mapped onto the plate surface as shown in Figure 5. The results of sensors effectiveness were also found to be similar for both sensor voltage time and frequency domain analyses. It can be observed from Figure 5 that the highest sensor effectiveness is at the root of the cantilever plate. The effectiveness reduces gradually toward the plate's axis of symmetry and the free end. Clearly, the highest sensor effectiveness occurs at the corners of the root of the cantilever plate, which agrees well with the published work [19] where the optimal locations of two sensor/actuator pairs were found at the corners of a cantilever plate. The Figure also shows the optimal locations

of the six s/a pairs located at the root of the plate and distributed symmetrically about the plate's axis of symmetry.

7.3 Validation of results

Results from the proposed method were obtained and compared with published results for optimal locations of collocated s/a pairs for active vibration reduction of a cantilever plate. It was shown that similar locations were obtained with greatly reduced computational effort. Also, the flexibility and effectiveness of the proposed method were tested to investigate asymmetrical dynamic plates (type-II and type-III) under external force and base excitations. The optimal locations were then used to place collocated s/a pairs for active vibration reduction and their effectiveness determined.

7.3.1 Optimal placement

First case study: single vibration mode

According to the methodology in Section 5, the optimal placement of ten s/a pairs was determined for the cantilever plate to suppress the first mode of vibration. Figure 6 shows the distribution of the peak of the output sensor voltage at the first natural frequency and their percentage effectiveness. It is shown from the figure that the optimal locations of the ten sensors is distributed symmetrically at the root of the cantilever plate (type-I). In this case study, the optimal locations of the ten s/a pairs were found to be similar to the optimal distribution obtained by Darivandi et al as shown in Figure 7 using the gradient-based optimization technique [16]. Figure 6 shows that the optimal locations obtained by Darivandi et al using genetic algorithms are significant different and hundreds of further generations are required to converge to those using gradient-based optimization technique.

Second case study: five vibration modes

Figure 8 (a) shows the distribution of the average percentage sensor effectiveness mapped on the surface of the cantilever plate to suppress the first five modes of vibration. The optimal placement of six sensors on a cantilever plate were chosen based on the ranking from Step 4 in Section 5, as shown in Figure 8(a). The mode weighting factor was taken as unity for all the first five modes of vibration. Figure 8 (b) shows the optimal placement of six sensors located by Han and Lee for the same cantilever plate based on gramian observability as an objective function to suppress the first five modes of vibration [9]. The optimal locations of the six sensors of the present work are shown in Figure 8 (a). They agree with the published work shown in Figure 8 (b) at four sensor locations and are different at two locations.

Table 3 shows more analyses carried out for the optimal sensor configurations in Figure 8. The table shows the contribution of the average percentage sensor effectiveness for each single mode and for all modes of vibration. Generally, the two optimal sensor configurations achieved comparable high values of sensor effectiveness for all modes of vibration except for the fifth mode, while the configuration of present method performed better. In Table 3, the numbers of s/a pairs and the total s/a pairs that are actively involved, respectively in each individual and all modes of vibration according to equations (17) and (18) are presented. It can be seen that the optimal placement of the present methodology offers more active s/a pairs in all the six modes of vibration in comparison with [9].

Also, it can be observed from the Table that the average percentage effectiveness of the two methods for the fifth mode is lower than that of the other modes. Using the present method, the distribution of the active s/a pairs on each mode can be controlled by selecting different mode weighting factor, β , for each mode according in equation (16). Thus, a high

percentage sensor effectiveness and number of active s/a pairs can be achieved for the desired mode of vibration by choosing a greater β , while others are smaller than one as explained in Section 7.3.4.

Table 4 shows a comparison study of the computation effort for the present study with published studies. The elapsed time shown in the Table was divided into two parts, i.e., the first part for determining structural natural frequencies and mode shapes using finite element method and the second part for optimizing computational effort. This elapsed time was not considered for most studies but just number of iterations and generations required for convergence to the optimal solution. It can be observed from the Table that the present method based frequency domain analysis requires much lower computational effort with only one cycle of calculation and elapsed time of only 22 seconds to get the optimal s/a locations. This comparison indicates that the methodology developed in this study holds great potential to solve both small and large-scale structures with lower computational effort to get the optimal sensor/actuator location.

7.3.2 Optimal sensor/actuator placement for asymmetrical dynamic structures

The optimal placement of six s/a pairs was studied for the asymmetrical dynamic plates (type-II and type-III) under external force excitation based on frequency domain analysis. Figure 9 (a, b, and c) show the distribution of the average sensor output voltage over the type-II plate for the first three modes of vibrations. It can be seen from the Figure that the sensor voltage is asymmetrically distributed around the plate axes as a result of asymmetrical plate boundary conditions. The optimal locations of the six s/a pairs were determined based on the average percentage of sensor effectiveness calculated for the six modes as shown in Figure (d). The Figure shows that the output voltage and the percentage effectiveness for the sensors

located close to the fixed ends are higher than others, among which the output voltage and percentage effectiveness for the sensor at locations 01, 10 and 91 are higher than the sensors located at positions 11, 61 and 81.

Figure 10 (a, b, and c) show the distribution of the sensor output voltage for the first three modes of vibration and the average percentage of sensors effectiveness is shown in Figure 10 (d) for the type-III plate. It can be observed from the Figure that the distribution is also asymmetric due to the T-shape beam stiffeners. The optimal locations of the s/a pairs for the type-III plate are also different from those of other types due to the effects of stiffeners.

7.3.3 *Optimal placement under base excitation*

In this section, the placement of s/a pairs is investigated for the type-III plate under base excitation instead of external force excitation. Structure base excitation was simulated in ANSYS finite element package by exciting all the fixed finite element nodes of the plate in the thickness direction. The ability to determine optimal locations of s/a pairs for simple and complex structures under base excitation is another advantageous feature of the present method, which is useful when it is difficult to choose an ideal location on a complex structure to apply an external force excitation. This test was applied to the type-III plate and compared with the results for the same structure under external force excitation. Figure 11 (a, b, c and d) show the output sensor voltage and the average percentage effectiveness distribution of the plate. In comparison with Figure 10, it can be seen that the results for the plate subject to external force excitation and base excitation agree with each other well.

7.3.4 *Activation of mode weighting factor*

The results in Sections 7.3.1 - 7.3.3 were obtained using mode weighting factor of 1.0 in equation 16. In this case study, the mode weighting factors, β , for the optimal placement were varied to test the flexibility of the placement method when the structure experiences a known internal or external excitation at or close to one or more natural frequencies. The other modes of vibration are less important but should also be taken into account. This can be dealt with by increasing the mode weighting factor of the strongly excited modes.

Figure 12 shows the optimal locations of six s/a pairs and the distribution of the average sensor percentage effectiveness using frequency response analysis for the asymmetrically stiffened plate under base excitation. The distribution of the average percentage sensor effectiveness and the location of the optimal six s/a pairs were determined using a mode weighting factor of 3.75 for the first mode (Figure 12.a), the third mode (Figure 12.b) and the fourth mode (Figure 12.c), while a mode weighting factor of 0.25 for all other five modes. Another new case study was investigated by locating one s/a pair at a location of 100% sensor effectiveness with unity weighting factor for each mode as shown in Figure 12 (d).

Table 5 shows a comparison study for five cases to calculate the average percentage sensor effectiveness for the optimal six s/a pairs at each mode and the total number of active s/a pairs. The optimal placement of six s/a pairs for the first case study in the Table 5 was located according to the previous Section 7.3 (Figure 11d). The last case study is a new placement which located one s/a pair at a position of 100% percentage sensor effectiveness at each mode (Figure 12d). It can be observed from Table 5 that the average percentage sensor effectiveness is 63.2, number of active s/a pairs is 22.75 and the effectiveness distribution at each mode for the first case study is higher and better performed than the last case study. The

results show that the present method gave better performance than the locating one s/a pairs at optimal effectiveness of each mode.

Also, Table 5 shows the effects of the activations of mode weighting factor for the first, third and fourth modes at second, third and fourth case study, respectively. It can be noticed from Table 5 that the average percentage sensor effectiveness are greater at these modes compared to the first case study, but causes slight reduction for the other less important modes and average . The use of mode weighting factor provides greater flexibility and an additional useful feature of the present method.

7.3.5 Active vibration reduction

The active vibration reduction of the first six modes was investigated using optimal linear quadratic control scheme for the type-III stiffened plate bonded with six s/a pairs located optimally as shown in Figure 13. A sinusoidal excitation voltage of $50\sin \omega_i t$ was applied to the actuators located at the positions of high sensor effectiveness 41, 70, 15, 50, 24 and 29 as shown in Figure 13 to actuate the stiffened plate at the 1st, 2nd, 3rd, 4th, 5th and 6th modes, respectively. These actuator locations were chosen due to their high sensor effectiveness at each mode in order to actuate the stiffened plate efficiently at the resonance modes.

A Matlab m-file and a Simulink model for active vibration reduction were built based on the model explained in Sections 3 and 4 using optimal linear quadratic control with weighting matrices of 10^8 for Q and 10^0 for R . Figures (14-16) show the results of transient and steady state time responses of the open loop sensor voltage (OLSV), closed loop sensor voltage (CLSV), actuator feedback voltage (AFBV) and external disturbance voltage (EXDV) of $50\sin\omega t$ at the first, third and sixth mode of vibration.

It was found a large percentage vibration reduction at the steady state closed loop control of 97.3%, 95%, 97.6%, 96.7%, 97.2% and 98.6% at the first six modes, respectively. These results demonstrate the effectiveness of the placement method in finding the optimal placement of piezoelectric s/a pairs for simple and complex structures.

Also, Figures (14-16) show a high speed response of vibration detection by sensors and attenuation by actuators at the transient zone. It can be observed from the Figures that the vibration sensing and attenuation started 0.001 seconds after the external disturbance was applied. This indicates that the optimal locations of the six s/a pairs on the type-III stiffened plate determined by this study are highly effective for vibration sensing and suppression.

CONCLUSION

In this study, an efficient method was developed to determine the optimal distribution of segmented sensors covering a single surface of a whole structure under external force or structure base excitations. The optimal sensor location was selected on the basis of maximum sensor output voltage and their average percentage effectiveness. This method reduces the number of candidate solutions to a single optimal solution, and therefore has great potential to apply to both small and large-scale structures.

The flexibility and effectiveness of the method were tested by investigating symmetrical and asymmetrical dynamic structures to find the optimal s/a distribution. The method was applied to a symmetrical cantilever plate and validated through comparisons with published work. It was then applied to more complex asymmetrical dynamic structures. The computational elapsed time of the present method and the number of iteration to find the optimal solution were found to be much lower than those reported in literature. The present method has an additional feature that allows increasing the percentage of sensor

effectiveness at an important mode by using an above unity mode weighting factor of that mode.

Finally, the proposed method is shown to give excellent active vibration reduction for a complex structure (an asymmetrically stiffened plate) in all of the first six vibration modes using the six optimally located sensor/actuator pairs.

The present method has demonstrated great flexibility in determining the global optimal distribution of s/a pairs for simple and complex structures under external force or structure base excitations by using time or frequency domain analysis. The present method has also great potential to be used to investigate small and large-scale structures with low computational effort.

The effect of uncertainties on the optimal sensor placement was not investigated in this study, However, It was found that the optimized sensor locations are not sensitive to a small change of the structural damping properties. Further investigations are required to study the uncertainties associated with other parameters.

ACKNOWLEDGMENT

The authors at Lancaster University are grateful to the EPSRC for financial support (EP/K020080/1).

REFERENCES

- [1] Lim, Y. H., 2003, "Finite Element Simulation of Closed Loop Vibration Control of a Smart Plate under Transient Loading," *Smart Materials and Structures*, vol. 12, no. 2, pp. 272–286.
- [2] Balamurugan, V., and Narayanan, S., 2010, "Finite Element Modeling of Stiffened Piezolaminated Plates and Shells with Piezoelectric Layers for Active Vibration Control," *Smart Materials and Structures*, vol. 19, no. 10, p. 105003.
- [3] Daraji, A. H., and Hale, J. M., 2014, "Active Vibration Reduction by Optimally Placed Sensors and Actuators with Application to Stiffened Plates by Beams," *Smart Materials and Structures*, vol. 23, no. 11, p. 115018.
- [4] Ramesh Kumar, K., and Narayanan, S., 2007, "The Optimal Location of Piezoelectric

- Actuators and Sensors for Vibration Control of Plates,” *Smart Materials and Structures*, vol. 16, no. 6, pp. 2680–2691.
- [5] Kondoh, S., Yatomi, C., and Inoue, K., 1989, “The Positioning of Sensors and Actuators in the Vibration Control of Flexible Systems,” *Japan Society of Mechanical Engineering*, vol. 55, no. 513, pp. 1206–1214.
- [6] Devasia, S., Mcressi, T., Paden, B., and Bayo, E., 1992, “Piezoelectric Actuator Design for Vibration Suppression: Placement and Sizing,” *Journal of Guidance, Control and Dynamics*, vol. 16, no. 5, pp. 859–864.
- [7] Zhang, H., Lennox, B., Zhang, H., Goulding, P. R., and Leung, A. Y. T., 2000, “A float-encoded Genetic Algorithm Technique for Integrated Optimization of Piezoelectric Actuator and Sensor Placement and Feedback Gains,” *Smart Materials and Structures*, vol. 9, no. 4, pp. 552–557.
- [8] Sadri, A. M. Wright, J. R., and Wynne, R. J., 1999, “Modelling and Optimal Placement of Piezoelectric Actuators in Isotropic plates Using Genetic Algorithms,” *Smart Materials and Structures*, vol. 8, no. 4, pp. 490–498.
- [9] Han, J. H., and Lee, I., 1999, “Optimal Placement of Piezoelectric Sensors and Actuators for Vibration Control of a Composite Plate Using Genetic Algorithms,” *Smart Materials and Structures*, vol. 8, no. 2, pp. 257–267.
- [10] Peng, F., 2005, “Actuator Placement Optimization and Adaptive Vibration Control of Plate Smart Structures,” *Intelligent Material Systems and Structures*, vol. 16, no. 3, pp. 263–271.
- [11] Liu, W., Hou, Z., and Demetriou, M. a., 2006, “A computational Scheme for the Optimal Sensor/Actuator Placement of Flexible Structures Using Spatial H_∞ measures,” *Mechanical Systems and Signal Processing*, vol. 20, no. 4, pp. 881–895.
- [12] Bruant, I., Gallimard, L., and Nikoukar, S., 2010, “Optimal Piezoelectric Actuator and Sensor Location for Active Vibration Control Using Genetic Algorithm,” *Sound and Vibration*, vol. 329, no. 10, pp. 1615–1635.
- [13] Montazeri, A., Poshtan, J., and Yousefi-Koma, A., 2008, “The Use of ‘Particle Swarm’ to Optimize the Control System in a PZT Laminated Plate,” *Smart Materials and Structures*, vol. 17, no. 4, p. 45027.
- [14] Rao, A. K., Natesan, K., Bhat, M. S., and Ganguli, R., 2008, “Experimental Demonstration of H_∞ control Based Active Vibration Suppression in Composite Fin-Tip of Aircraft Using Optimally Placed Piezoelectric Patch Actuators,” *Intelligent Material Systems and Structures*, vol. 19, pp. 651–669.
- [15] Dutta, R., Ganguli, R., and Mani, V., 2011, “Structures Swarm Intelligence Algorithms for Integrated Optimization of Piezoelectric Actuator and Sensor Placement and Feedback gains,” *Smart Materials and Structures*, vol. 20, no. 10, p. 105018.
- [16] Darivandi, N., Morris, K., and Khajepour, A., 2013, “An Algorithm for LQ Optimal Actuator Location,” *Smart Materials and Structures*, vol. 22, no. 3, p. 35001.
- [17] Ogata, K., 1990, *Modern Control Engineering*. Second Edition. New Jersey: Prentice-Hall, Englewood Cliffs.
- [18] Papadimitriou, C., 2004, “Optimal Sensor Placement Methodology for Parametric Identification of Structural Systems,” *Sound and Vibration*, vol. 278, no. 5, pp. 923–947.
- [19] Padoin, E., Fonseca, J. S. Perondi, E. A., and Menuzzi, O., 2015, “Optimal Placement of Piezoelectric Macro Fiber Composite Patches on Composite Plates for Vibration Suppression,” *Solids and Structures*, vol. 12, no. 5, pp. 925–947.

Figure Captions List

- Fig.1. (a) Total number of candidate solutions for a plate discretized to one hundred positions to optimize locations of piezoelectric sensors from one to one hundred; (b) y-axis in log scale.
- Fig.2. Cantilever smart plates bonded with one hundred piezoceramic sensors sequentially numbered from left to right and down to up
- Fig.3. Distribution of sensors output voltage based on time domain analysis at steady state and frequency domain analysis for the 1st, 2nd and 5th resonance modes of type-I plate
- Fig.4. Sensors output voltage time response at transient zone for the first mode, plate type-I
- Fig.5. Distribution of average percentage sensor effectiveness and selection of the optimal locations of six s/a pairs on the surface of type-I plate
- Fig.6. Optimal distribution of ten s/a pairs on type-I plate using present method
- Fig.7. Optimal distribution of ten s/a pairs on type-I plate [16]
- Fig.8. Optimal distribution of six sensors on cantilever plates
- Fig. 9 (a, b and c) Optimal distribution of sensors voltage for the 1st, 2nd and 3rd modes; (d) average sensor effectiveness for the first six modes and the location of the optimal six s/a pairs for type-II plate
- Fig. 10 (a, b and c) Optimal distribution of sensors voltage for the 1st, 2nd and 3rd modes; (d) average sensor effectiveness for the first six modes and the location of the optimal six s/a pairs for type-III plate under external force excitation.
- Fig. 11 (a, b and c) Optimal distribution of sensors voltage for the 1st, 2nd and 3rd modes; (d) average sensor effectiveness for the first six modes and the location of the optimal six s/a pairs for type-III plate under base excitation.
- Fig. 12 Distribution of average sensor effectiveness for the first six modes of type-III plate under base excitation, a) $\beta_1=3.75$, b) $\beta_3=3.75$, c) $\beta_4=3.75$, $\beta_i=0.25$ for all other five modes for the three cases, d) sensors located at maximum percentage effectiveness for each mode $\beta_i=1$ for all the six modes.
- Fig. 13. Optimal s/a location and locations of external voltage disturbance actuation at first six modes of the stiffened plate
- Fig. 13. Optimal s/a location and locations of external voltage disturbance actuation at first six modes of the stiffened plate
- Fig.14. Transient and steady state time responses of the s/a at the optimal location 01 as a result of applied external voltage on actuator at location 41 and at the 1st mode

Fig. 15. Transient and steady state voltage time responses of the s/a at the optimal location01 as a result of applied external voltage on actuator at location 15 at the 3rd mode

Fig. 16. Transient and steady state time responses of the s/a at the optimal location 11 as a result of applied external voltage on actuator at location 29 at the 6th mode

Table Captions List

Table 1 Plate and piezoelectric properties

Table 2 Natural frequencies

Table 3 Comparison of percentage effectiveness for the optimal sensor locations

Table 4 Comparison of the computation effort in optimization

Table 5 Mode weighting factor effects on optimal sensor effectiveness

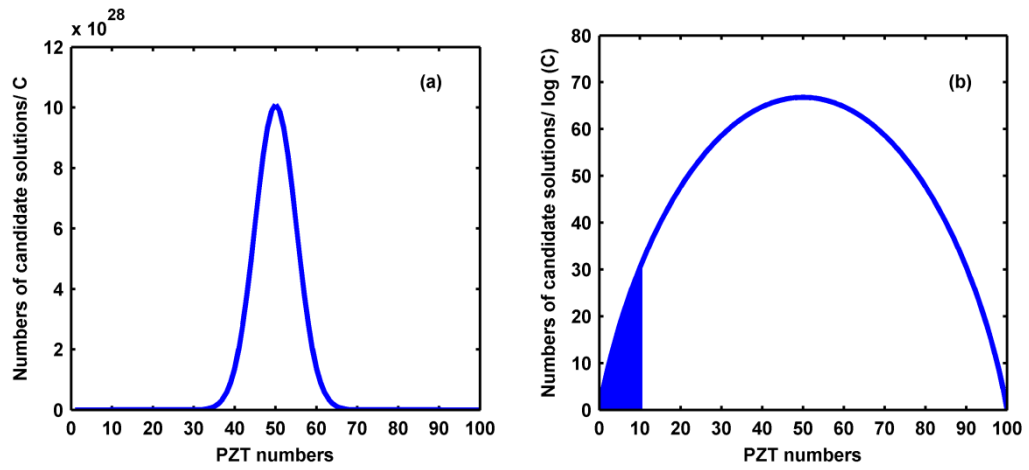
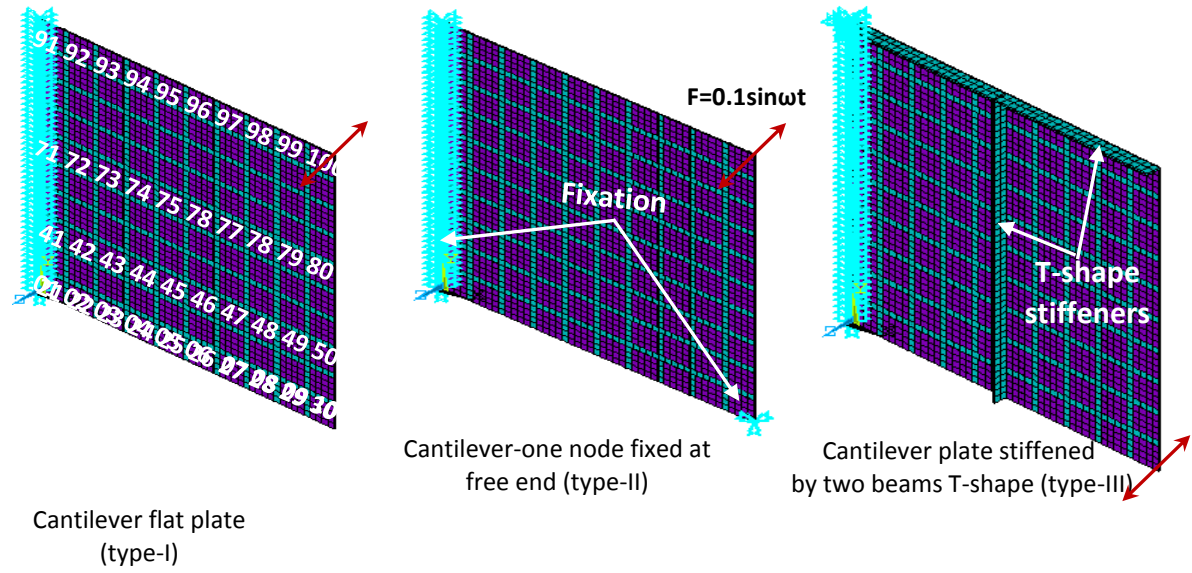
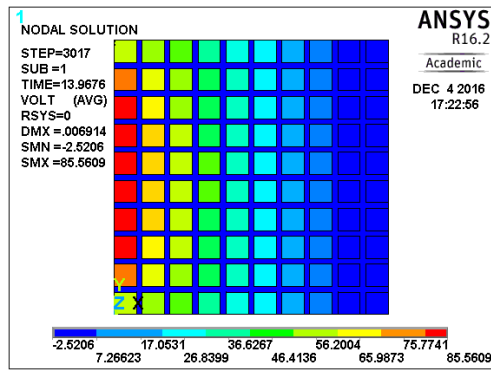


Fig.1. (a) Total number of candidate solutions for a plate discretized to one hundred positions to optimize locations of piezoelectric sensors from one to one hundred; (b) y-axis in log scale.

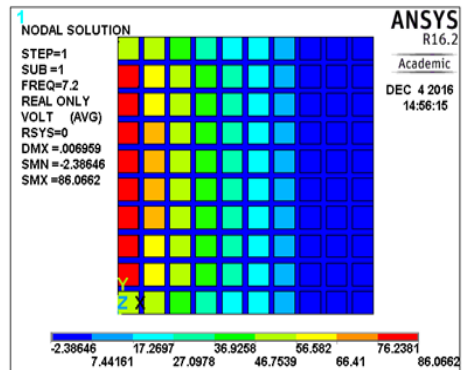


Cantilever flat plate
(type-I)

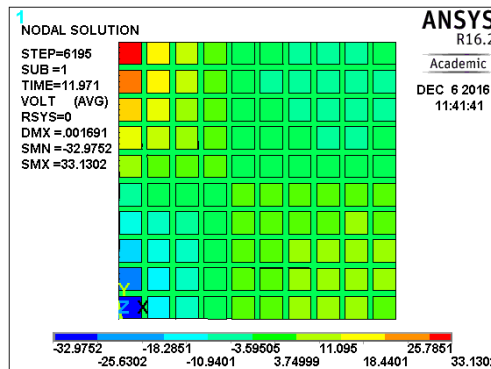
Fig.2. Cantilever smart plates bonded with one hundred piezoceramic sensors sequentially numbered from left to right and down to up



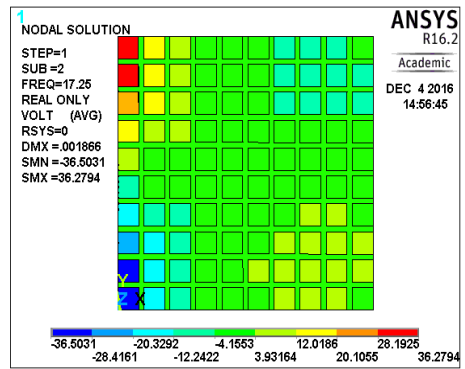
1st mode time domain



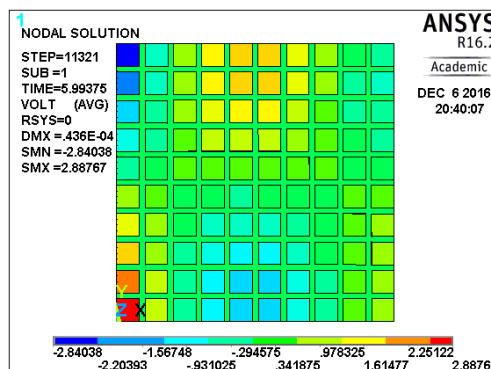
1st mode frequency domain



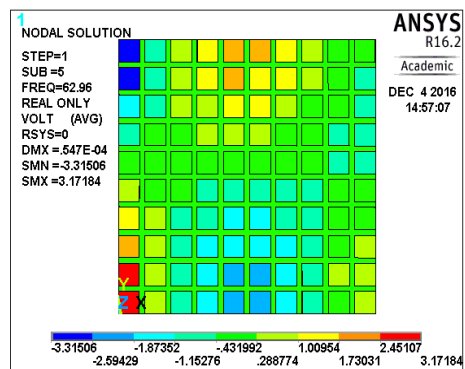
2nd mode time domain



2nd mode frequency domain



5th mode time domain



5th mode frequency domain

Fig.3. Distribution of sensors output voltage based on time domain analysis at steady state and frequency domain analysis for the 1st, 2nd and 5th resonance modes of type-I plate

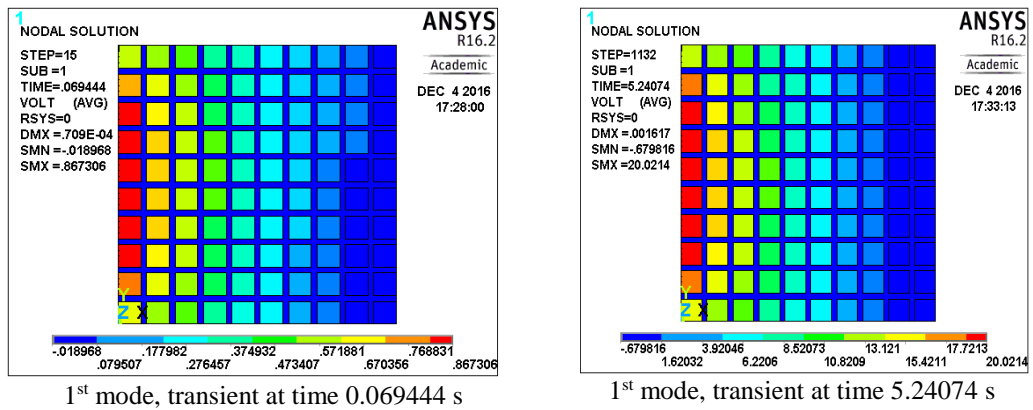


Fig.4. Sensors output voltage time response at transient zone for the first mode, plate type-I

76.3	37.2	22.1	30.4	34.0	34.0	27.3	16.8	10.1	6.80
74.7	38.3	23.7	32.9	37.1	37.4	30.8	19.7	11.6	9.2
68.1	36.4	23.5	33.2	38.0	38.9	33.2	23.3	17.4	15.7
60.1	32.7	22.0	31.8	37.1	38.3	34.0	25.8	21.6	20.8
51.0	28.1	19.5	28.7	34.0	35.3	32.7	28.1	22.4	22.1
52.6	28.2	20.5	30.5	36.3	37.8	34.7	28.3	21.0	20.4
59.3	31.8	22.6	32.3	37.5	38.7	34.4	26.4	18.6	20.0
68.6	34.5	23.7	32.4	36.5	37.0	31.4	21.8	14.9	16.1
71.3	37.6	23.6	31.0	34.0	33.8	27.1	16.6	9.9	9.9
74.9	36.3	21.9	28.2	30.4	29.7	23.2	15.7	10.1	6.7

Fig.5. Distribution of average percentage sensor effectiveness and selection of the optimal locations of six s/a pairs on the surface of type-I plate

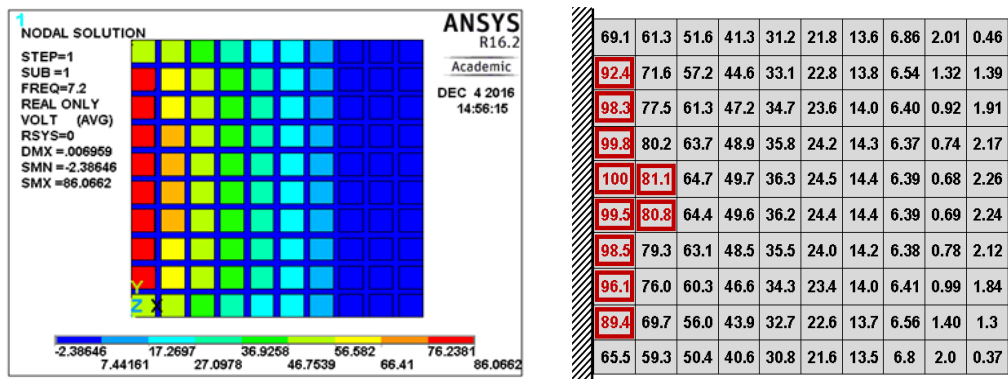


Fig.6. Optimal distribution of ten s/a pairs on type-I plate using present method

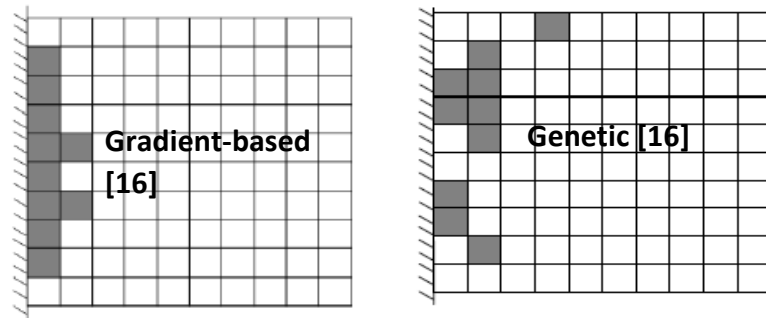
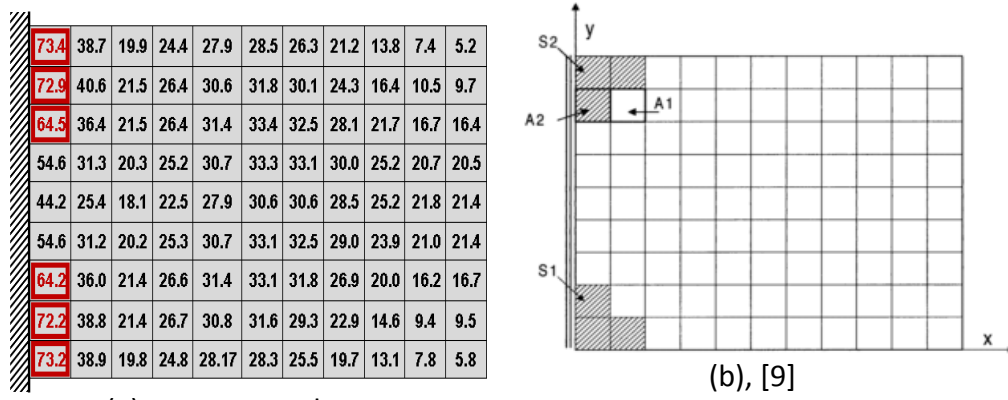


Fig.7. Optimal distribution of ten s/a pairs on type-I plate [16]



(a), Present work

Fig.8. Optimal distribution of six sensors on cantilever plates

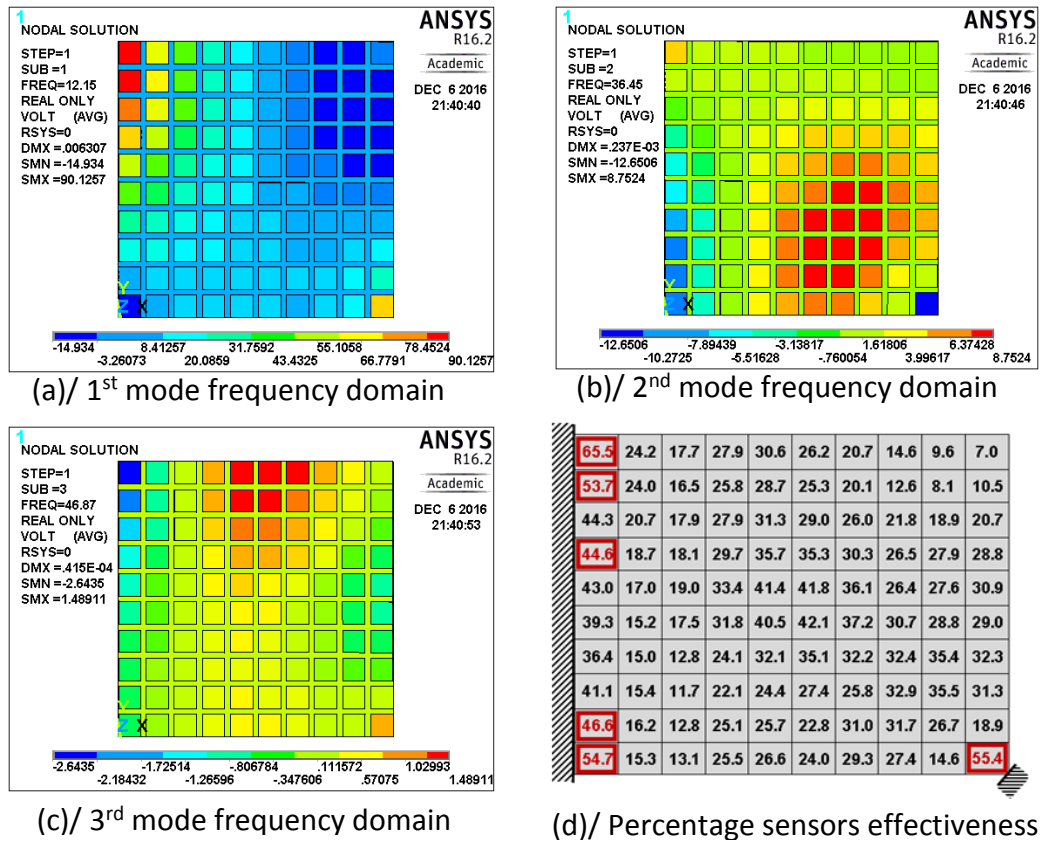


Fig. 9 (a, b and c) Optimal distribution of sensors voltage for the 1st, 2nd and 3rd modes; (d) average sensor effectiveness for the first six modes and the location of the optimal six s/a pairs for type-II plate

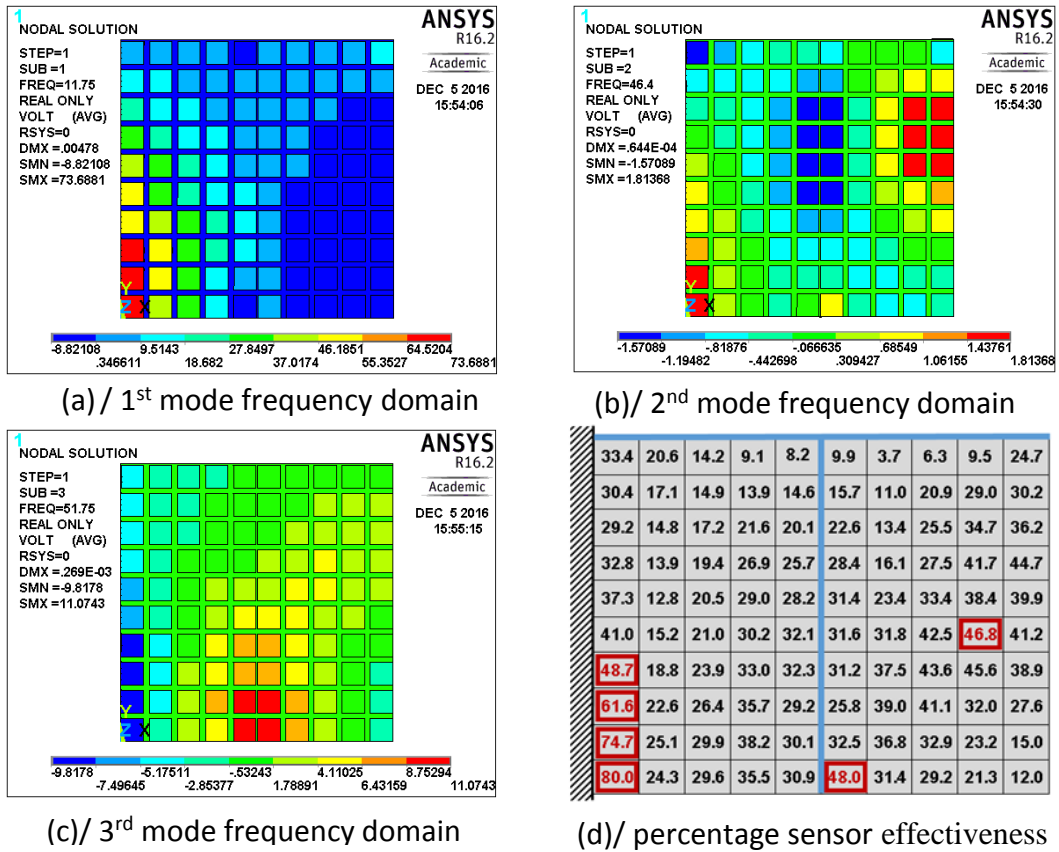
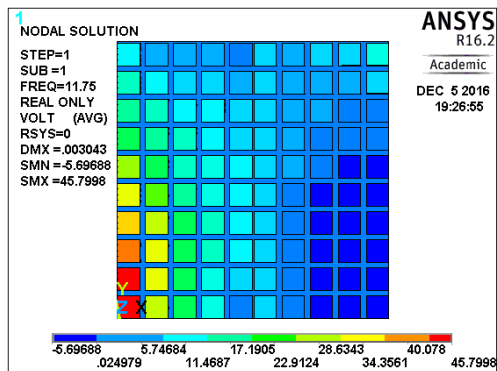
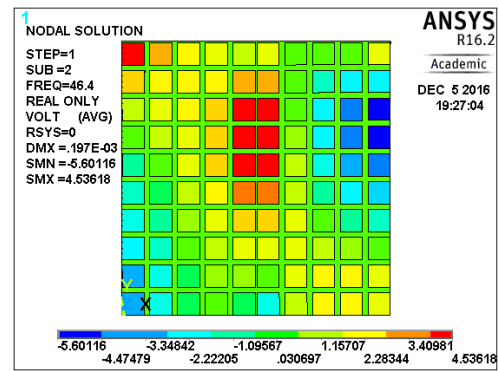


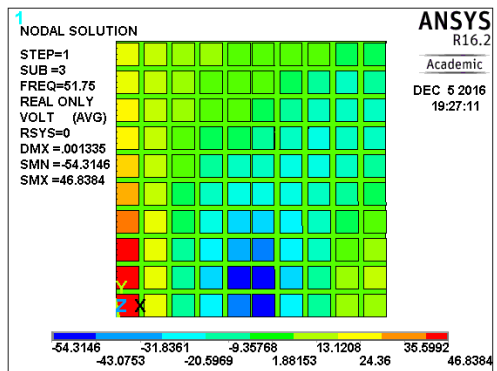
Fig. 10 (a, b and c) Optimal distribution of sensors voltage for the 1st, 2nd and 3rd modes; (d) average sensor effectiveness for the first six modes and the location of the optimal six s/a pairs for type-III plate under external force excitation.



(a)/1st mode frequency domain



(b)/ 2nd mode frequency domain



(c)/ 3rd mode frequency domain

33.4	20.7	15.0	10.5	8.4	9.6	4.2	7.5	10.0	20.3
30.6	17.2	15.4	13.6	14.1	13.8	12.1	21.6	30.1	31.7
30.7	16.2	16.6	20.4	18.7	18.7	17.1	27.0	34.3	37.2
33.9	14.9	21.2	28.3	25.5	25.4	21.4	35.5	40.5	44.4
42.0	13.5	25.7	34.2	30.3	30.5	28.8	43.5	46.2	38.9
47.2	16.3	28.9	37.7	31.8	33.2	35.7	45.3	43.8	38.7
55.8	20.4	30.7	38.7	30.1	32.7	40.8	41.5	33.6	35.0
67.3	24.3	34.8	40.9	28.1	30.0	43.8	41.1	22.7	23.3
79.2	26.8	38.7	43.5	31.4	35.5	44.4	38.9	22.8	15.8
83.3	26.2	37.6	42.6	32.7	47.7	40.8	40.5	27.5	12.9

(d)/ percentage sensors effectiveness

Fig. 11 (a, b and c) Optimal distribution of sensors voltage for the 1st, 2nd and 3rd modes; (d) average sensor effectiveness for the first six modes and the location of the optimal six s/a pairs for type-III plate under base excitation.

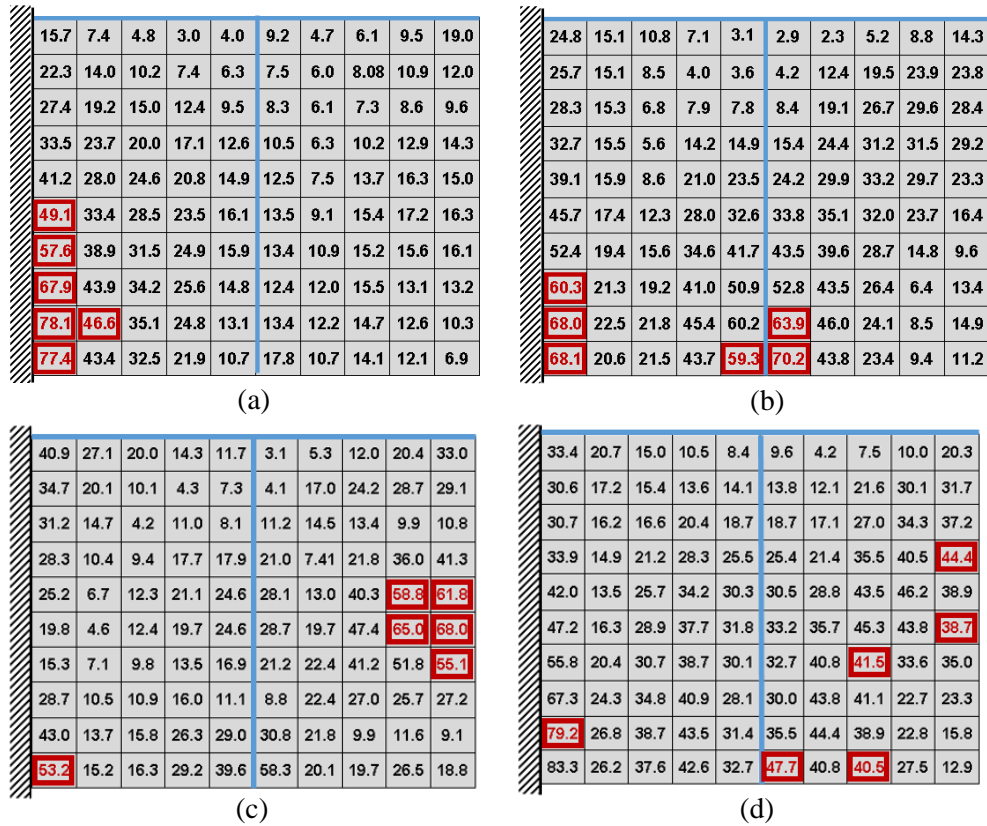


Fig. 12 Distribution of average sensor effectiveness for the first six modes of type-III plate under base excitation, a) $\beta_1 = 3.75$, b) $\beta_3 = 3.75$, c) $\beta_4 = 3.75$, $\beta_i = 0.25$ for all other five modes for the three cases, d) sensors located at maximum percentage effectiveness for each mode $\beta_i = 1$ for all the six modes.

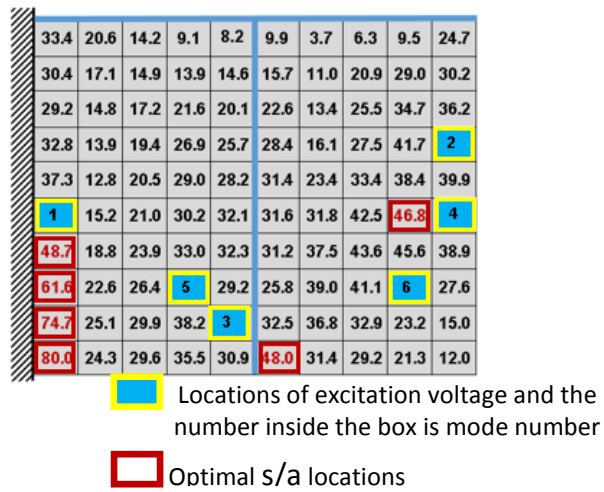


Fig. 13. Optimal s/a location and locations of external voltage disturbance actuation at first six modes of the stiffened plate

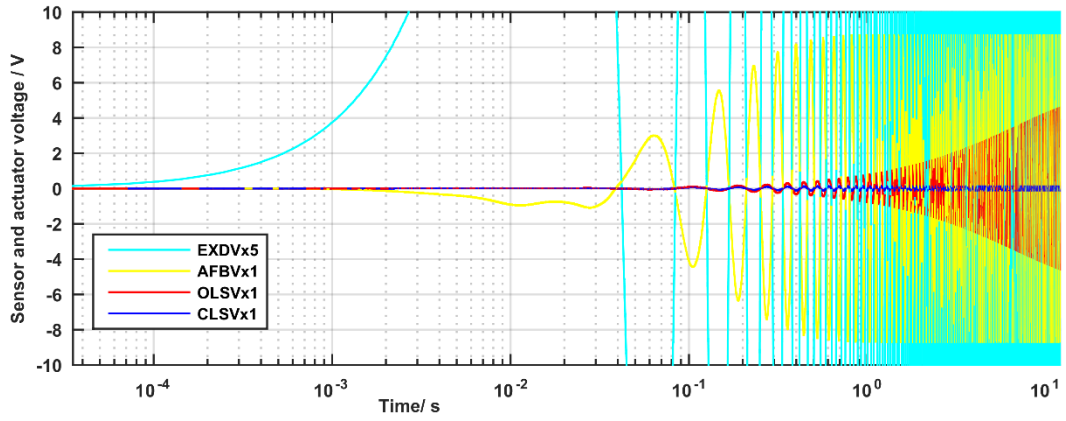


Fig.14. Transient and steady state time responses of the s/a at the optimal location 01 as a result of applied external voltage on actuator at location 41 and at the 1st mode

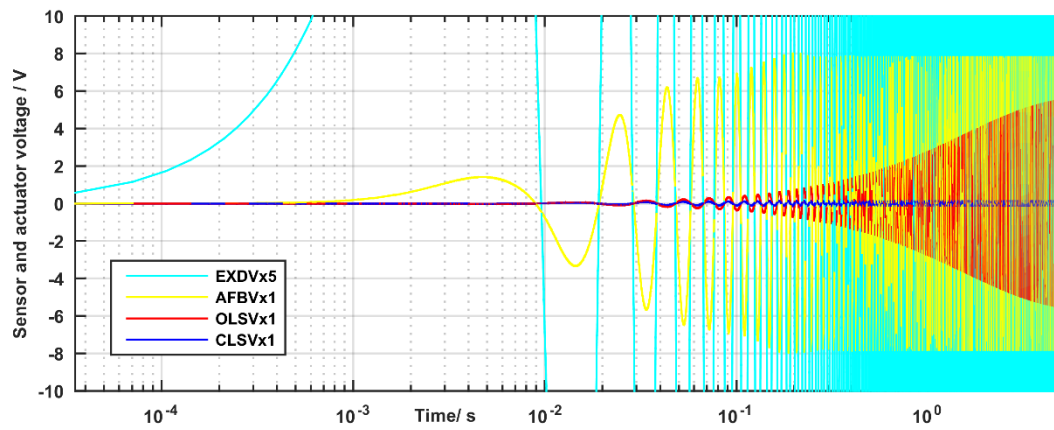


Fig. 15. Transient and steady state voltage time responses of the s/a at the optimal location01 as a result of applied external voltage on actuator at location 15 at the 3rd mode

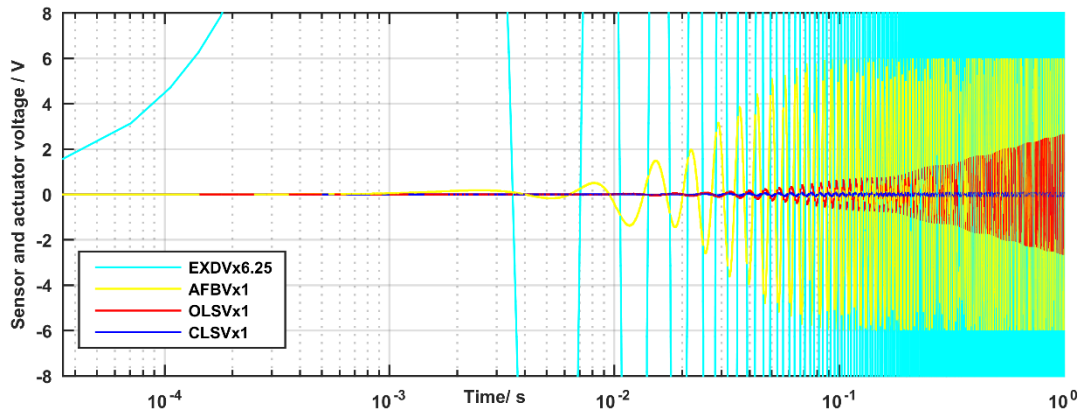


Fig. 16. Transient and steady state time responses of the s/a at the optimal location 11 as a result of applied external voltage on actuator at location 29 at the 6th mode

Table 1 Plate and piezoelectric properties

Properties	Plate type I, II	Plate type III	Piezoelectric PIC255
Modulus, GPa	210	210	-----
Density, Kg/m ³	7810	7810	7180
Poisson's ratio	0.3	0.3	-----
Thickness, mm	1.9	1.9	0.5
Stiffener thickness ,mm	-----	3	-----
Length, width, mm	490,490	483,493	40,40
e_{31}, e_{32}, e_{33} , C/m ²	-----	-----	-7.15, -7.15, 13.7
$C_{11}^E, C_{12}^E, C_{13}^E$, GPa	-----	-----	123, 76.7, 70.25
$C_{22}^E, C_{23}^E, C_{33}^E$	-----	-----	123.11, 70.2, 97.11
$C_{44}^E, C_{55}^E, C_{66}^E$	-----	-----	22.8, 22.2, 23.1
μ_{33}^σ F/m	-----	-----	1.5×10^{-8}

Table 2 Natural frequencies

Plate type	Frequency (Hz)					
	1 st	2 nd	3 rd	4 th	5 th	6 th
Type-I	7.2	17.25	43.66	55.71	62.96	109.66
Type-II	12.15	36.45	46.87	62.02	94.42	118.10
Type-III	11.75	46.40	51.75	88.40	135.0	141.70

Table 3 Comparison of percentage effectiveness for the optimal sensor locations

Optimal sensor locations	Average percentage effectiveness for all six sensors						Total number of active s/a pairs for each case study
	1 st	2 nd	3 rd	4 th	5 th	Average	
Present work	82.9	81.97	88.19	79.7	17.5	70.0	0.7×6×5=21
Han and Lee [9]	68.9	81.4	71.5	72.9	13.0	61.5	0.61×6×5=18
Number of active s/a /present study	4.97	4.91	5.29	4.78	1.05	4.2/mode	

Table 4 Comparison of the computation effort in optimization

Reference/ method	Structure dimension mm	sensor and actuator/ mode	Number of candidates solutions	Number of iterations to get the optimal solution	Elapsed time for natural frequency and mode shape/s	Elapsed time for optimization/s
[3]/GA	500×500	10/6	1.73×10^{13}	250×10^3	9**	4065**
[4]/GA	500×500	10/6	1.73×10^{13}	75×10^3	---	---
[9] /GA	220×180	6/5	11.2×10^9	50×10^3	---	---
[11]/GA	900×450	4/4	0.277×10^7	100×10^3	---	---
[15] /GA	300×380	3/8	1.05×10^7	800	---	---
[16] /GA	500×500	10/1	1.73×10^{13}	---	---	4.44333×10^4
[13]/PS	1000×1000	2/33	2×10^6	4000	---	---
Present work/ type-I	490×490	10/1	$1.73 \times 10^{13} - 10^{29}$	1	11.5**	14.5**
Present work/ type-III	483×493	6/6	$11.9 \times 10^8 - 10^{29}$	1	13**	22**

Note: ** refers to the program run on the same computer properties , --- unavailable
 GA refers to Genetic Algorithms and PS refers to Particle Swarm

Table 5 Mode weighting factor effects on optimal sensor effectiveness

Mode weighting factor β	Average percentage sensor effectiveness for all six s/a pairs							Active s/a pairs	Figure number
	1 st mode	2 nd mode	3 rd mode	4 th mode	5 th mode	6 th mode	Average		
Unity / Section 7.3.3	63	61	72.5	46.4	70.0	66.5	63.2	22.75	11 (d)
$\beta_1=3.75$, others 0.25	81.8	52.3	64.8	23.9	75.7	62.9	60.2	21.6	12 (a)
$\beta_3=3.75$, others 0.25	51.2	43.4	86.7	47.8	59.1	57.6	57.6	20.7	12 (b)
$\beta_4=3.75$, others 0.25	24.8	64.3	28.4	83.0	40.3	45.2	47.6	17.1	12 (c)
One s/a pair at optimal effectiveness of each mode	23.7	52.9	46.6	56.7	53.8	58.3	48.6	17.5	12 (d)